

See discussions, stats, and author profiles for this publication at: <https://www.researchgate.net/publication/377983796>

Investigating Isogyres in Ferrofluids and Horocycles from Parlaseric Circle in a Ferroc cell

Article in *Journal of Optics and Photonics Research* · February 2024

DOI: 10.47852/bonviewJOPR42022329

CITATIONS

0

READS

5

2 authors, including:



Alberto Tufaile

University of São Paulo

110 PUBLICATIONS 590 CITATIONS

SEE PROFILE

RESEARCH ARTICLE

Journal of Optics and Photonics Research

yyyy, Vol. XX(XX) 1–5

DOI: 10.47852/bonviewjOPR42022329

Investigating Isogyres in Ferrofluids and Horocycles from Parlaseric Circle in a Ferroc cell



BON VIEW PUBLISHING

Alberto Tufaile^{1,*} and Adriana Pedrosa Biscaia Tufaile¹

1 School of Arts, Sciences and Humanities, University of São Paulo, Brazil

Abstract: This study explored the complex relationship between magnetic fields and light polarization in thin films of ferrofluid. Utilizing techniques such as polarized light imaging, multipolar expansion, and Mueller matrix formalism, this work investigated the formation of isogyres, which are distinct patterns observed when polarized light passes through the ferrofluid under various magnetic field configurations. The analysis revealed that the alignment of nanoparticles in response to the magnetic field resulted in the formation of a diffraction grating, influencing light polarization. Through the application of Stokes vectors and Mueller matrices, we gained insights into the complex interplay between magnetic fields and optical properties. The experiment presents the evolution of isogyres from straight lines to parabolas under the influence of a hexapolar magnetic field. The Mueller matrix effectively represented the magnetic field's impact on polarized light, highlighting dark regions corresponding to isogyres. We also report the formation of some patterns related to atmospheric optics and their analogy with the formation of patterns of the parlaseric circle and the luminous horocycle.

Keywords: isogyres, luminous horocycles, parlaseric circle, ferroc cell, ferrofluid

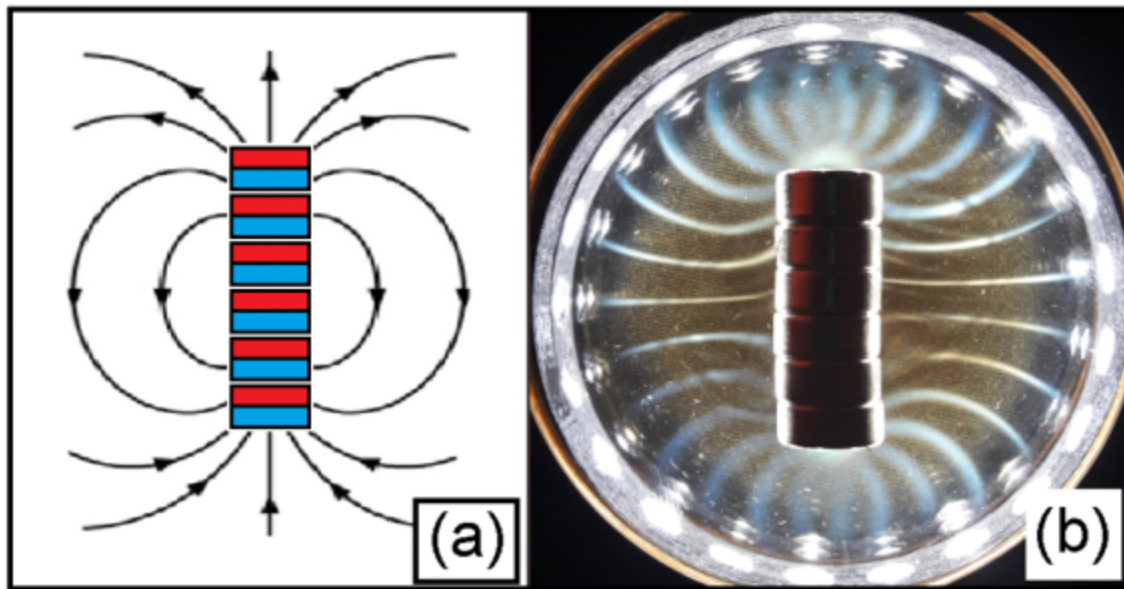
*Corresponding author: Alberto Tufaile, School of Arts, Sciences and Humanities, University of São Paulo, Brazil. Email: tufaile@usp.br

1. Introduction

The Ferroc cell is a device that produces patterns when exposed to a magnetic field while interacting with a light source (Tufaile et al., 2019) [1]. Consisting of two plates made of glass, with a thin layer of ferrofluid between them, the Ferroc cell is complemented by an encircling LED strip, as it is shown in Figure 1. When a magnet is brought close, the ferrofluid reacts to the magnetic field, altering the path of light passing through it. The main reason for this effect is because ferrofluids exhibit the ability to form reversible two-dimensional (2D) ordered structures in a thin film when exposed to external magnetic fields. These structured films result from the alignment or arrangement of superparamagnetic nanoparticles influenced by the magnetic field. Significantly, these ordered thin films possess the capacity to control the propagation of light (Haas & Adams, 1975; Mendelev & Ivanov, 2004; Ivanov & Zubarev, 2020) [2-4]. Essentially, the alignment of nanoparticles induced by the external magnetic field creates a periodic structure that influences the transmission of light, mimicking the behavior of an optical grating, an optical device that diffracts light into specific directions, as it is shown in Figure 2(a). Furthermore, these devices are capable of altering the polarization of light, as we can see in Figure 2(b). This capacity to control and polarize light holds potential applications in diverse optical and photonic devices.

Figure 1

A stack of six magnetic disks placed on a Ferroc cell. In (a) the magnetic field diagram and in (b) an image of the pattern of this magnetic field in a Ferroc cell.

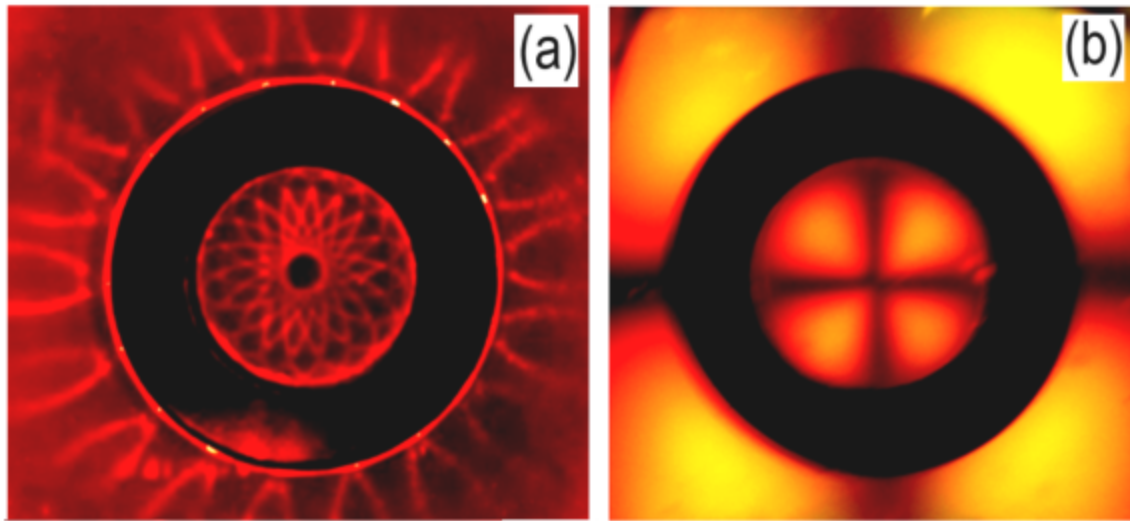


In this way, the understanding of the interaction between magnetic fields and light polarization in these thin films could lead to the creation of magneto-optical devices, offering possibilities for manipulating light in areas such as optical communication, sensing, and imaging (Hornig et al., 2003; Martinez et al., 2005; Candiani et al., 2011; Thakur et al., 2011; Zu et al., 2012a; Zu et al., 2012b; Li et al., 2014; Li et al., 2021; Cennamo et al., 2020; Gao et al., 2022; Chen et al., 2023)[5-15]. The study of particle orientation in ferrofluid thin films holds promise for applications in materials science and nanotechnology, potentially influencing the development of materials with tailored properties (Dave et al., 2020; Chen et al., 2018)[16, 17]. Another aspect is that the exploration of chiral properties in these films may open avenues in chiral optics and photonics, leading to innovative applications in sensors, filters, or other optical devices (Fan et al., 2021)[18]. Additionally, the controllable manipulation of light polarization in a Ferrocell might find applications in biomedical applications, offering enhanced capabilities for medical applications (Minuti et al., 2022; Shokrollahi, 2013) [19, 20]. Furthermore, the observed flexibilization of patterns under different magnetic field configurations could have implications for optical data storage, contributing to more adaptable and efficient technologies (Gu et al., 2014) [21]. Overall, a profound understanding of magnetic fields and light polarization in ferrofluid thin films has the potential to revolutionize technology and science with novel applications, such as the technology involving display applications. The ability of ferrofluids to respond to magnetic fields and control the orientation of nanoparticles offers opportunities for creating dynamic and new types of tunable displays. The ferrofluid-based displays could be used in applications where the flexibility and adaptability of the display content are desired, similar to some aspects of liquid crystal displays (LCDs). By manipulating the magnetic field, it's possible to control the alignment of nanoparticles in the ferrofluid, influencing the transmission of light and polarization. This property can be leveraged in display technologies to achieve features such as variable transparency, color modulation, and dynamic patterns.

Ferrocell technology holds potential for solar panels by incorporating magnetic field-responsive patterns, enhancing performance. These patterns can be directly applied to solar cells or used as coatings, optimizing sunlight absorption. Real-world testing is essential to evaluate energy production, durability, and longevity. Implementation requires thorough research and collaboration to balance enhanced performance with cost-effective, scalable production. The gained insights may inform the design of photonic materials for integrated photonics, benefiting applications like signal processing and telecommunications (Mansuori et al., 2015) [22].

Figure 2

Example of patterns obtained with the Ferrocell under the action of a magnetic ring illuminated by a ring of LEDs and with polarized light. Image of a magnetic ring on a Ferrocell in (a). In (b), luminous pattern of polarized light for this same system. Understanding the pattern with isogyres brings new information about this system.



It's crucial to acknowledge that the realization of these applications depends on further research, development, and the practical implementation of findings, and because of this, in this study, we delve into the generation of isogyres, which in the domain of polarized light refers to a specific pattern of dark bands that materializes when polarized light traverses the samples, like the ferrofluid, when exposed to a magnetic field, undergoes structural transformations impacting the polarization of transmitted light. The distinctive arrangement and rotation of these dark bands offer valuable clues, shedding light on the optical and structural characteristics of the ferrofluid and the structural alterations induced by the magnetic field.

Our research establishes a link between isogyres from crystal optics (Samlan et al., 2016) [23] with ferrofluids, demonstrating their manifestation as dark cross patterns in the passage of light through the ferrofluid with specific optical properties. The concept of isogyres comes from conoscopy. A conoscopic system, also known as a conoscopic interferometer, is an optical instrument used for studying and analyzing the optical properties of materials, particularly birefringent materials. In this conoscopic system, light is typically passed through a birefringent crystal or sample. The emerging light forms an interference pattern, revealing information about the optical characteristics of the material, such as refractive indices, birefringence, and optical axis orientation. Here, we are using this technique to study structures formed inside the ferrofluid subjected to a magnetic field, using an orthoscopic system. Orthoscopy and conoscopy are both techniques used in microscopy, particularly in the field of crystallography, to study the optical properties of materials.

Within the realm of crystal optics, an isogyre manifests as a dark cross pattern observed when light traverses a crystal with distinct optical properties, like the dark cross shown in Figure 2(b). The term "Maltese cross" is employed to depict this dark cross formed by isogyres. The emergence of isogyres is a result of the interaction between polarized light and the crystal. The dark cross aligns with the orientations of both the polarizer and the analyzer. Along this cross, the state of polarization of the light remains constant during its passage through the crystal. The two isogyres intersect at the visual field's center, coinciding with the optic axis of the uniaxial crystal. The presence and characteristics of isogyres offer valuable insights into the optical properties of the crystal and the behavior of polarized light within it, and the examination of isogyres has found widespread application in crystal-related research (Kamb, 1958; Victor & Beyer, 1973; Berry et al., 1999; Kompaneitsev, 2006; Samlan et al., 2016) [24-28]. In our experiment, the distinctive arrangement and rotation of the dark bands provide valuable information about the optical characteristics of the ferrofluid and the structural alterations induced by the magnetic field.

In addition to exploring isogyres, we will further investigate certain aspects of diffraction in the Ferrocell using phenomena explained by the Geometric Theory of Diffraction (GTD) (Keller, 1962) [29] and drawing parallels with atmospheric optics. One such phenomenon is the parhelic circle (Conover, 2015) [30], generated by ice crystals of micrometer-sized, similar to the microneedles formed by nanoparticles in the Ferrocell in the presence of a magnetic field. The parhelic circle, resulting from light scattering in ice crystals, and its tabletop demonstration counterpart, the parlaseric circle (Keller, 1962; Conover, 2015; Fitzgerald, 2019) [29, 30, 31], arising from light scattering in foams at Plateau borders, produce reflective points known as sundogs and laser dogs (Conover, 2015) [30], respectively, or luminous dogs in general. This occurs due to the hexagonal geometric structures in ice crystals and triangular prisms at Plateau borders (Tufaile & Tufaile, 2015) [32]. The absence of luminous dogs in the luminous horocycle observed in the Ferrocell is related to the irregular internal structures of ferrofluid micro-needles, distinguishing them from ice crystals or Plateau borders.

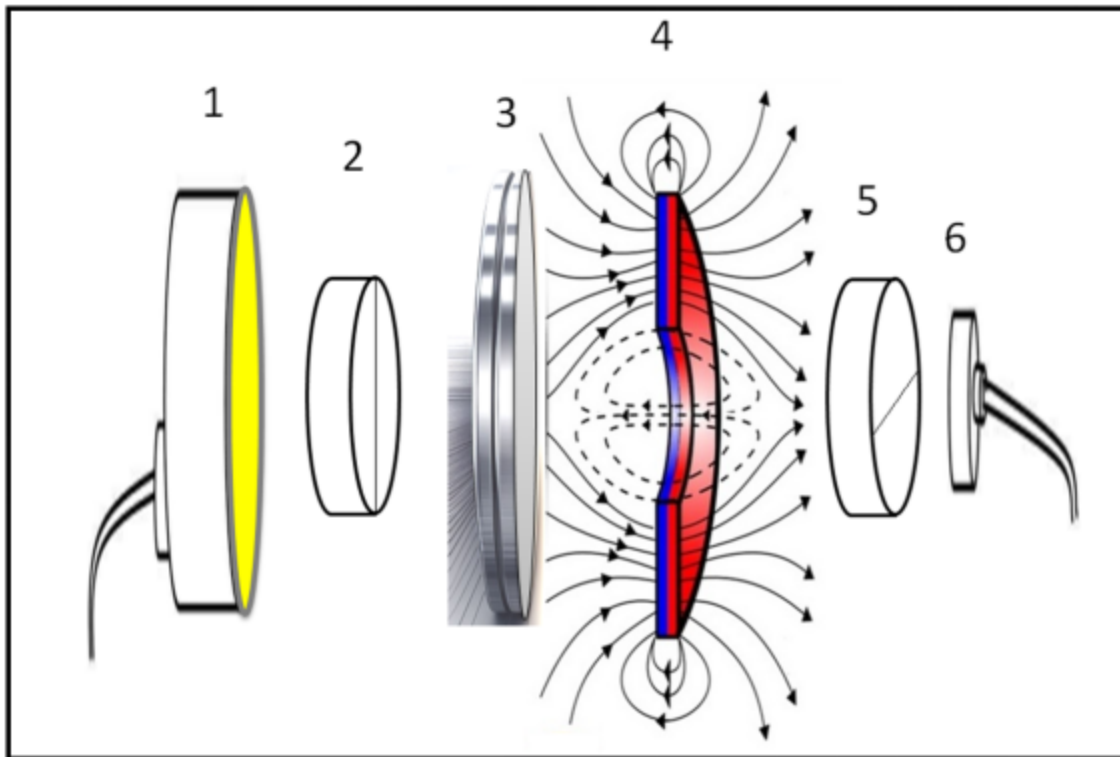
In the next section we present our experimental apparatus, after that we discuss the existence of isogyres in the polarization patterns. Next we also present the observation of the Parlaseric Circle phenomenon, a luminous ring linked to diffraction, generated by light scattering in foams or soap bubbles using the Ferrocell. The observed diffraction circle projections reveal five luminous points, with the leftmost point representing the laser beam interacting with the Plateau border, and the other points representing laser dogs, reflections of the laser beam. Using a Ferrocell to observe this luminous pattern and applying a magnetic field generates images of luminous Horocycles. These horocycles predominantly form in areas with intense light signals, particularly where there is a strong laser reflection from the Plateau border. At the end, we do our final remarks in the conclusion.

2. Experimental Apparatus and Mathematical Tools

In this polarization study, we employed polarimetry as our experimental technique. Polarimetry involves measuring and analyzing the polarization state of light, where light's oscillations occur in various directions perpendicular to its propagation. Key devices, like polarizers and analyzers, play a crucial role. A polarizer permits only light with specific polarization to pass through, while an analyzer, placed after the sample, measures the light's polarization after interaction. This setup enables exploration of diverse polarization states, such as linear, circular, and elliptical, contributing to our investigation of the thin ferrofluid film's polarization properties, because our goal is to understand its optical characteristics, examining nanoparticle distribution under different applied magnetic field configurations, like it is shown in the diagram of Figure 3.

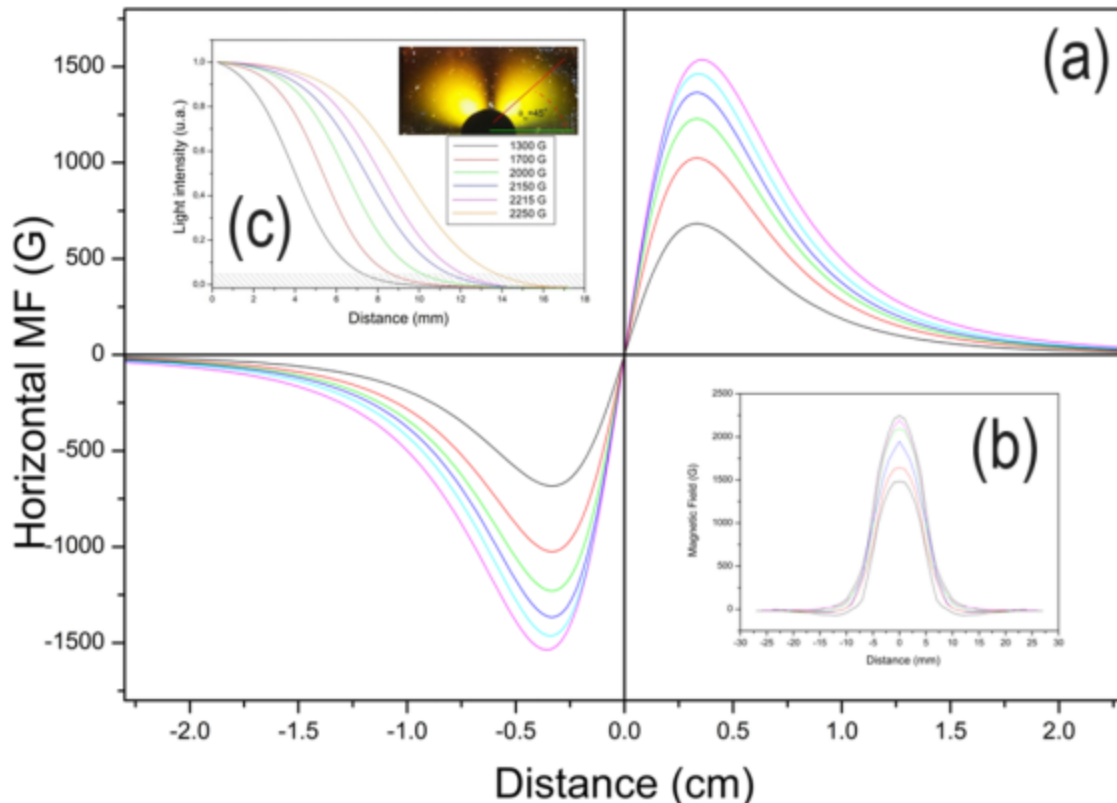
The experiment employs EFH1 (Ferrotec) ferrofluid characterized by a saturation magnetization of 440 G and 10 nm single-domain iron oxide nanoparticles. This ferrofluid solution is sandwiched between two glass plates, each exhibiting a thickness variation of approximately $1\ \mu\text{m}$, resulting in a thin film with an overall thickness of around $10\ \mu\text{m}$. The ferrofluid demonstrates a response time on the order of 200 ms, and the scattering pattern swiftly disappears upon the removal of the magnetic field. At very low magnetic fields, the ferrofluid exhibits isotropic behavior. Neodymium super magnets, positioned in close proximity to the Ferrocell, serve as the source of the magnetic field, with the maximum magnetic field strength generated by these magnets in the order of 2000 G in this experiment.

Figure 3
Diagram of the experimental apparatus. (1) Primary light source, (2) polarizer, (3) Ferrocell, (4) magnet generating the magnetic field, (5) analyzer, and light sensor (6).



To change the strength of the magnetic field, additional identical magnets are added atop the initial magnet, facilitating an increase in field strength. This configuration enables the utilization of magnetic field strength as an independent variable within this system, as it is shown in Figure 4. Measurements of the field components are taken from the central point on one face of the magnetic cylinder and extend linearly from this point using a Hall sensor on the surface of the plane where the Ferrocell is positioned. This particular field setup is referred to as monopolar, as the Ferrocell predominantly touches one of the "charges" of a magnetic dipole. The polarization of light is highly dependent on the intensity of the magnetic field, as the magnetic field alters the density of lines in the diffraction grating created by nanoparticles. Typically, in the context of light polarization, the light intensity exhibits a linear increase with the magnetic field intensity for given angles between the polarizer and the field, reaching saturation at magnetic field values around 1500 gauss, as can be inferred from the graphs in Figure 4. With respect to wavelength, several tests conducted with UV and infrared light led us to some conclusions. Regarding the wavelength, the phenomenon is primarily observed in the visible light range due to certain Ferrocell construction factors, but the magnetic field does not significantly affect the wavelength. The presence of glass plates in the cell affects the wavelength in the UV range. The fluid dispersing the nanoparticles, such as oil or water, influences the effects in the infrared range. So far, we have observed that the most significant results occur relatively uniformly in the visible range. This does not rule out the possibility of future investigations being conducted based on wavelength.

Figure 4
Plots of applied magnetic field intensities and their effects on the formation of light patterns. In (a) horizontal magnetic field of a dipole, (b) magnetic field of a monopole, and in (c) light intensity of polarized light for different values of magnetic field.



To analyze some physical properties of the patterns observed in this paper, we use the Stokes vector, with Mueller matrices operating on such vectors, to have measurable parameters with real values obtained with appropriate optical instruments (Tufaile & Tufaile, 2022) [33]. The incident light is represented using a Stokes vector, and the resulting signal obtained when the Ferrocell interacts with this incident light is represented by another final Stokes vector. The Stokes parameters, denoted as I , Q , U , and V , form a 4×1 column vector S representing the components of the electric oscillations of light. This vector describes a complete state of polarization with the polar and azimuth angles, denoted as (θ, ϕ) , respectively. These parameters are correlated

with the Stokes vector S_{PP} observed in the patterns within a Ferroc cell, comprising six intensity values, namely I_P , I_S , I_{+45} , I_{-45} , I_R , and I_L , as outlined in our previous paper (Tufaile & Tufaile, 2022) [33].

$$S = \begin{bmatrix} I \\ Q \\ U \\ V \end{bmatrix} = \sqrt{\frac{\epsilon}{\mu}} \begin{bmatrix} E_{0\theta}E_{0\theta}^* + E_{0\phi\theta}E_{0\phi}^* \\ E_{0\theta}E_{0\theta}^* - E_{0\phi\theta}E_{0\phi}^* \\ -2R\theta E_{0\theta}E_{0\phi}^* \\ 2ImE_{0\theta}E_{0\phi}^* \end{bmatrix} \Rightarrow S_{PP} = \begin{bmatrix} I_P + I_S \\ I_P - I_S \\ I_{+45} - I_{-45} \\ I_R - I_L \end{bmatrix}. \quad (1)$$

Equation (1) presents the final vector, providing all the necessary components to describe the observed polarization state of light in this system. A visually insightful interpretation of the Stokes vector is to envision its relation to the S_i elements of the Poincaré sphere, particularly for a completely polarized light beam. In this graphical representation, the sphere's radius, denoted as S_0 , signifies the incident irradiance of the light beam. The difference in radiant energy flux per unit area, or irradiances, between the horizontal component I_P and vertical polarization component I_S is represented by S_x . The preference for $+45^\circ$ or -45° polarization is indicated by S_y , while S_z is associated with the impact of right or left circular polarization states affecting the light. Thus, any polarization state can be defined by the vector extending from the origin at the center of the sphere to a point on the surface of the Poincaré sphere. In this manner, every polarization state is determined by the vector extending from the center of the sphere to a point on its surface, as described by the following equation.

$$S_0^2 \geq S_x^2 + S_y^2 + S_z^2. \quad (2)$$

The Mueller matrix describes the Stokes vector after the interaction with matter, and the interaction between light and the sample for the case of the Mueller matrix and Stokes vector is represented by the linear transformation of an incident Stokes vector S_0 to an outgoing Stokes vector S_1 due to the 4×4 Mueller matrix M :

$$S_1 = M \cdot S_0 \Rightarrow S_1 = \begin{bmatrix} m_{11} & m_{12} & m_{13} & m_{14} \\ m_{21} & m_{22} & m_{23} & m_{24} \\ m_{31} & m_{32} & m_{33} & m_{34} \\ m_{41} & m_{42} & m_{43} & m_{44} \end{bmatrix} S_0. \quad (3)$$

In this way, analytical formulas for the Stokes vectors, ellipticity, and azimuth are derived for every point in the sample, perpendicular to the propagation direction, at the output of this system. These parameters facilitate a comprehensive depiction of the polarization state throughout the thin film of ferrofluid recorded in the image, which is used as our data.

The Mueller matrix functions as a mathematical tool to describe the alteration of polarized light when interacting with an optical system. In the experiment involving ferrofluid and a magnetic field, this matrix effectively demonstrates how the magnetic field affects polarized light, offering crucial insights into optical characteristics like polarization and intensity. The Mueller matrix, by representing and quantifying the magnetic field's impact on polarized light, proves instrumental in comprehending the relationship between magnetic fields and optical properties in the Ferroc cell experiment. The identification of dark regions, associated with zero values in the light intensity from Stokes parameters, provides a clear indication of the presence and characteristics of isogyres, enhancing our comprehensive understanding of this system.

There are three ways to observe the luminous patterns in the Ferroc cell. The first involves observing the pattern in the light source through the Ferroc cell, similar to how polarization patterns are examined. The second method is to pass a laser beam through the Ferroc cell and observe the resulting pattern on a screen when studying the diffraction of a laser beam. The third approach is to directly observe the luminous pattern within the Ferroc cell, as we will do in the case of the luminous horocycle. To record the image, we take photos of the observed system and analyze these images with appropriate software, such as Origin and Maple.

The key aspects of this experiment is that the alignment of nanoparticles in ferrofluid thin films, triggered by a magnetic field, significantly impacts light polarization. Ferrofluids contain superparamagnetic nanoparticles that, upon exposure to an external magnetic field, align themselves parallel to the field lines. This alignment creates ordered structures within the ferrofluid, resulting in a periodic arrangement of nanoparticles, and the aligned nanoparticles act as a diffraction grating. In the context of ferrofluids, the aligned nanoparticles form a grating-like structure that affects the propagation of light passing through the thin film. This grating alters the direction and intensity of the transmitted light, leading to changes in its polarization state. In this study, we explore the behavior of a ferrofluid diffraction grating influenced by a magnetic field. The magnetic field induces the alignment of nanoparticles, resulting in needle-shaped structures with distances between them on the order of tens of

micrometers. Commonly used for optical gratings, the optical range is between 100 nm and 10 μm . The distinct optical properties of ferrofluids under a magnetic field, forming structures with diffraction characteristics, raise the question of their wavelength range. The specified range (100 nm to 10 μm) covers the visible light spectrum (400 nm to 700 nm) and extends into the infrared region, encompassing a broader electromagnetic spectrum. However, practical limitations, such as the glass plates or the oil used as a liquid carrier for the iron nanoparticles covered by the surfactant, limit the device's operation to the visible wavelength range. As light interacts with the ordered structures created by the aligned nanoparticles, it undergoes diffraction, similar to the behavior of light passing through a traditional diffraction grating. The diffraction process influences the polarization of light, and the periodic arrangement of nanoparticles introduces a spatial modulation in the transmitted light. This modulation, in turn, contributes to changes in the polarization state of the transmitted light.

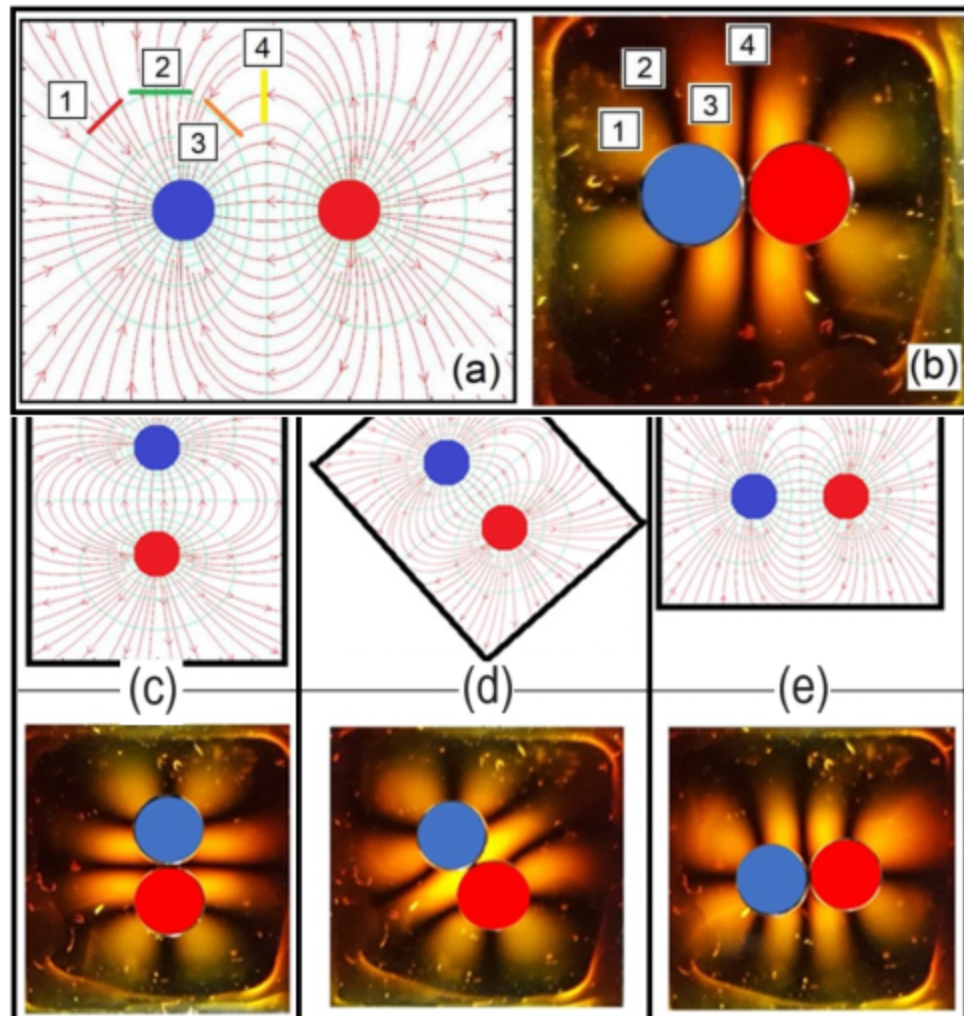
3. Exploring the Evolution of Isogyres

Let's establish the connection between the light at each point in the polarization pattern and its corresponding Stokes parameter in the scenario of a dipole magnetic field applied to the plane containing the thin ferrofluid film, as depicted in Figure 5, using the blue circles to represent the south pole and red for the north pole. As elucidated in our previous work (Keller, 1962) [29], ferrofluid particles align themselves with the applied magnetic field, akin to the formation of the depicted field lines in Figure 5(a). The polarization pattern with isogyres is shown in Figure 5(b).

In a system comprising a linear polarizer and linear analyzer, our results suggest that the polarization orientation is perpendicular to the magnetic field lines. Consequently, light polarization vectors parallel or perpendicular to either the input or output elements of the polarizer/analyzer system will be obstructed, resulting in dark regions within the polarization pattern, as illustrated in Figure 5(b). Points where the light polarization is at 45° relative to any of the elements of the polarizing/analyzer system will exhibit maximum light intensity. For angles between these two cases, the light intensity will vary in accordance with the projection on a trigonometric circle, characteristic of harmonic functions.

Figure 5

Relating magnetic field lines (a) of a magnetic dipole with patterns observed in Ferrocell in (b). Magnetic dipole p with different alignments and respective polarization patterns: (c) dipole aligned with the vertical, (d) dipole aligned diagonally, (e) dipole aligned with the horizontal.



When the magnetic field is rotated, it influences the alignment of particles within a material, as it is shown in Figures 5(c)-5(e), and the observable patterns formed by isogyres are subject to changes when the magnetic field is turned. The alignment of particles with the magnetic field is a crucial factor affecting these patterns, and variations occur as the magnetic field orientation is adjusted. Thoroughly analyzing this light pattern with a 90° counterclockwise rotation of Figures 5(c)-5(e), we can examine an axis traversing the north and south poles within the Ferroc cell plane. In cases where this axis aligns horizontally or vertically, a comparable isogyre pattern emerges, featuring eight illuminated regions—two flanking each pole. On the other hand, when the axis assumes a diagonal orientation, the pattern still comprises eight illuminated regions. However, it exhibits two prominent lobes along the diagonal perpendicular to the pole alignment axis, accompanied by three less intense lobes along the outer periphery of the poles.

By placing a magnetic bar that creates a dipolar field on the Ferroc cell, we will obtain the main lines of the isogyres of Figure 6. We begin by algebraically representing the magnetic field lines of this bar magnet with magnetic moment p . In cartesian coordinates (x, z) and polar coordinates (r, θ) , the equations for the dipole magnetic field lines B in the Ferroc cell plane are given by:

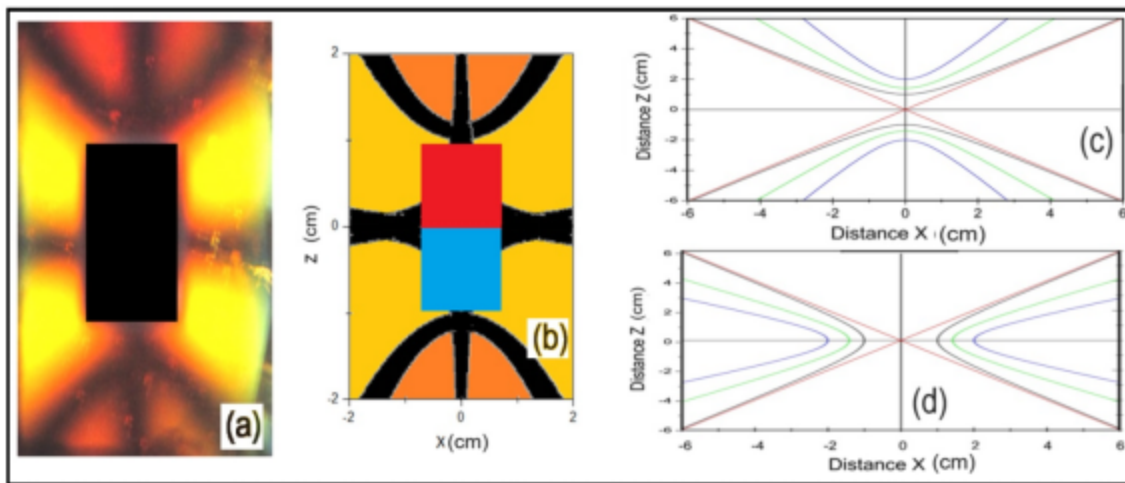
$$B_x = \frac{3pxz}{(x^2+z^2)^{5/2}} = \frac{3p \sin \theta \cos \theta}{r^3}, \quad (4)$$

$$B_z = \left[\frac{3z^2}{(x^2+z^2)^{5/2}} - \frac{1}{(x^2+z^2)^{3/2}} \right] = \frac{p(3 \cos^2 \theta - 1)}{r^3}. \quad (5)$$

Given this angular distribution of the field lines by Eqs. (4)-(5), the nanoparticles align with this field of a magnet bar that is shown in the image of the experiment in Figure 6(a) with its respective diagram shown in Figure 6(b). According to these equations, the concentration of isogyres must follow the lines represented in Figures 6(c)-6(d). Consequently, by rotating the magnetic field by 90° , we will have a rotation of the isogyres, as shown in Figure 6 (d) below Figure 6 (c). This rotation is evident during dipole rotation in Figures 5(c)-5(d). In regions with a weak magnetic field (less than 200 gauss), a diffraction grating does not form, leading to dark areas around the pattern.

Figure 6

In (a), represents the polarization pattern of a magnetic bar, while (b) presents a corresponding diagram. Hyperbolas depict isogyres projected onto the Ferroc cell, varying with distance from the magnetic dipole center relative to the y-axis. Isogyre lines aligning horizontally and vertically through the origin are also visible. In (c), with a vertical dipole orientation, and in (d), with a horizontal orientation, two red lines along the diagonals mark the limits for forming hyperbolas. Each color in the plots indicates different distances from the magnet in relation to the Ferroc cell plane in the Y direction.



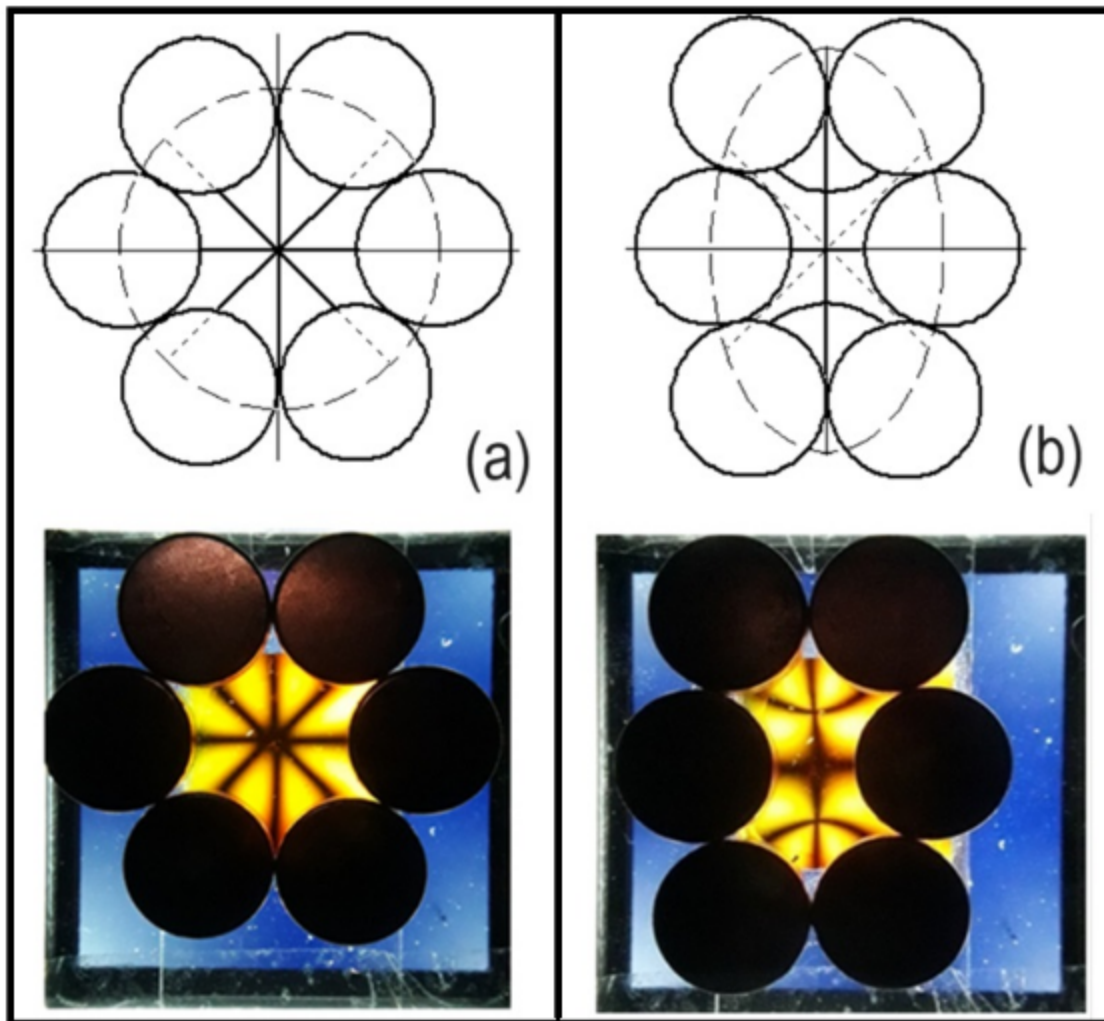
To show the impact of magnetic field intensity on the polarization of light, the diagrams represented in Figures 6 (c) and 6 (d) illustrate that the isogyre pattern can be changed, as each curve with a certain color is related to different configurations of the

magnetic field. The horizontal and vertical straight lines indicate the alignment of the magnetic field along the z-axis and x-axis, corresponding to one of the polarizers.

The plots depicted in Figure 6 prompt the question of how hyperbolas can undergo a transformation into straight lines in this particular scenario. To answer this question, we can use a hexapolar (sextupolar) field, illustrated in Figure 7. This approach is based on the concept of multipolar expansion, aiming to illustrate the effects of changes in a dipolar magnetic field through the use of an asymmetric sextupolar field. The luminous pattern obtained the sextupolar magnetic field simplifies the observation of isogyres at the center of the luminous pattern and their evolution based on adjustments to the magnet positioning. The symmetric sextupolar field, with four straight isogyres that intersect in the center in Figure 7 (a), presents the same configuration as the red and black lines in the diagrams in Figures 6(c) and 6(d). This pattern is reflected in the two black lines along the vertical and horizontal axes, as well as the two red lines on the diagonal, representing the limits of the hyperbolas from the dipole field.

Figure 7

Light polarization patterns of two configurations of a sextupolar magnetic field showing multipolar expansion observed by isogiral patterns. (a) Illustrates magnets symmetrically arranged in a circumference. In (b), magnets are positioned in an ellipse aligned vertically.

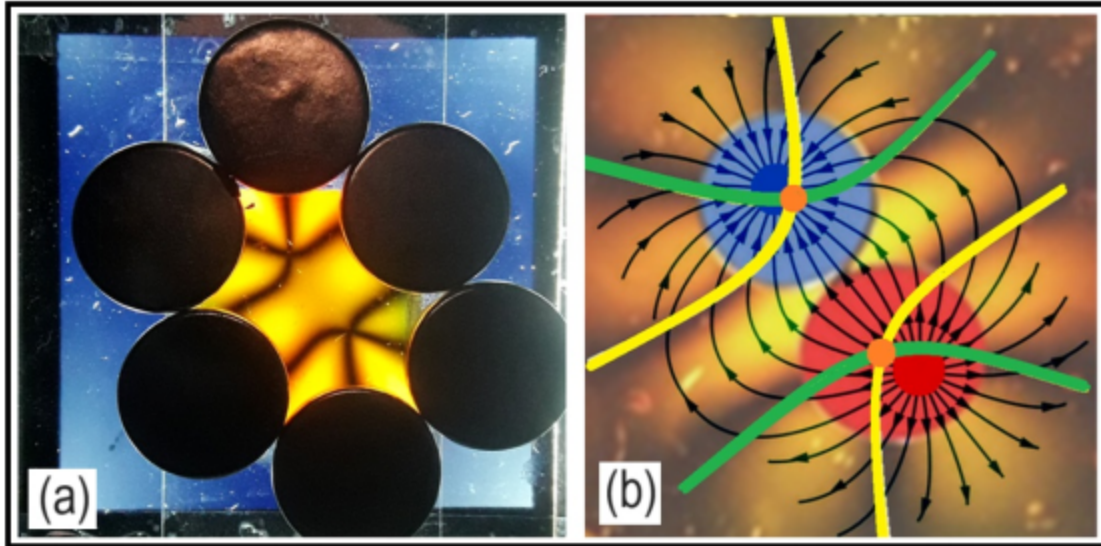


We can observe that by changing the applied magnetic field, these light patterns undergo a transformation in their shape in Figure 7. Initially, the isogyres in Figure 7(a) appear as straight lines, but when the magnetic field is modified, they evolve into parabolic shapes. Figure 7(b) exhibits a comparable pattern in the case of the dipolar magnetic field, indicating that this sextupolar magnetic field possesses a dipolar magnetic field (p) component oriented in the vertical direction.

Figure 8 depicts the visualization of isogyres using sextupolar and dipolar magnetic field configurations rotated 45° relative to the horizontal axis. When these magnetic fields exhibit symmetry in either horizontal or vertical directions and are rotated by 45°, four isogyres are formed. Two of these isogyres align at 90° (depicted in yellow), and the other two align at 0° (depicted in green). The intersection point of these isogyres occurs at the geometric center of each magnetic charge of the respective dipole, where the orientations cancel each other out.

Figure 8

Luminous pattern resulting from a sextupolar configuration with diagonal symmetry alignment, displaying exclusively curved isogyres in (a). The luminous pattern of a dipolar configuration with diagonal symmetry alignment is depicted in (b), accompanied by a diagram illustrating the magnetic field lines. Yellow lines signify alignment of the diffraction grating with the vertical, while green lines indicate alignment with the horizontal.



We can model the properties of light in these patterns using Mueller Matrices. The scenario involves a sextupolar magnetic field, which influences the alignment of nanoparticles in a ferrofluid, creating a diffraction grating. The goal is to represent this grating using a Mueller Matrix, which is a mathematical tool commonly employed in polarimetry to describe the transformation of polarized light as it interacts with optical elements. We need to represent the diffraction grating that will be created by the ferrofluid nanoparticles aligning to the hexapolar magnetic field with Mueller matrices, as is in our previous work (Tufailé & Tufailé, 2022) [33]. For the matrix representing an asymmetric sextupole, we have the following matrix:

$$M_1 = \frac{1}{2} \begin{bmatrix} 1.8 & m_{12} & m_{13} & 0 \\ m_{21} & m_{22} & m_{23} & 0 \\ m_{31} & m_{32} & m_{33} & 0 \\ 0 & 0 & 0 & 0 \end{bmatrix}, \quad (6)$$

where:

$$m_{12} = m_{21} = 0.8 \cos(\theta) + \cos(4\theta), \quad (7)$$

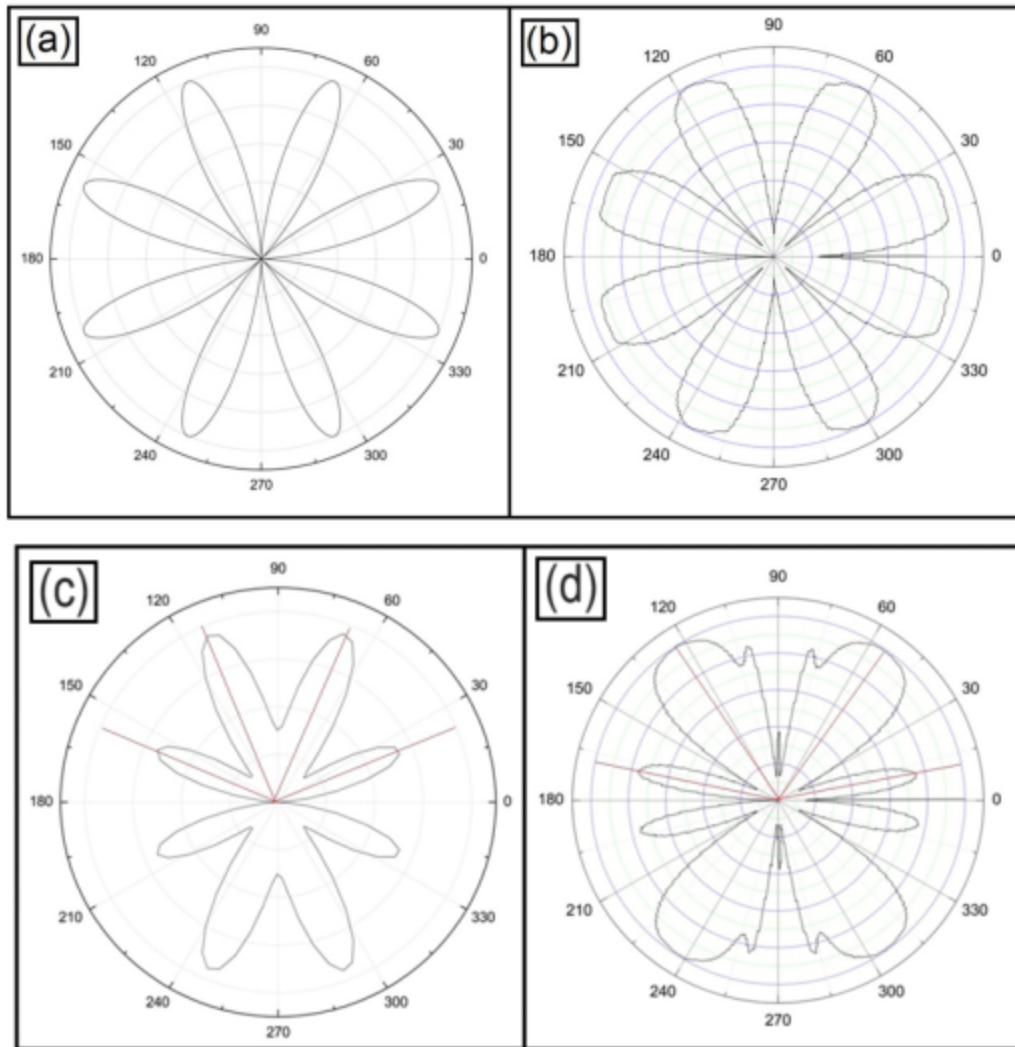
$$m_{13} = m_{31} = 0.8 \sin(\theta) + \sin(4\theta), \quad (8)$$

$$m_{23} = m_{32} = 0.8 \sin(\theta) + \cos(\theta) + \cos(4\theta) + \sin(4\theta), \quad (9)$$

$$m_{22} = m_{33} = 0.8 \cos(\theta)^2 + \cos(4\theta)^2. \quad (10)$$

Following this, we apply the Stokes vectors that act on this matrix to vertically polarized light and to an analyzer positioned after the ferrofluid. We will focus on the parameter I of the light intensity, specifically around the center of the light pattern.

Figure 9
Simulation illustration employing Stokes vectors and experimental outcomes showcasing light intensities of sextupolar fields with circular and elliptical configurations. Polar plots in (a) and (c) present the results obtained with our model, while polar plots in (b) and (d) display the corresponding experimental results.

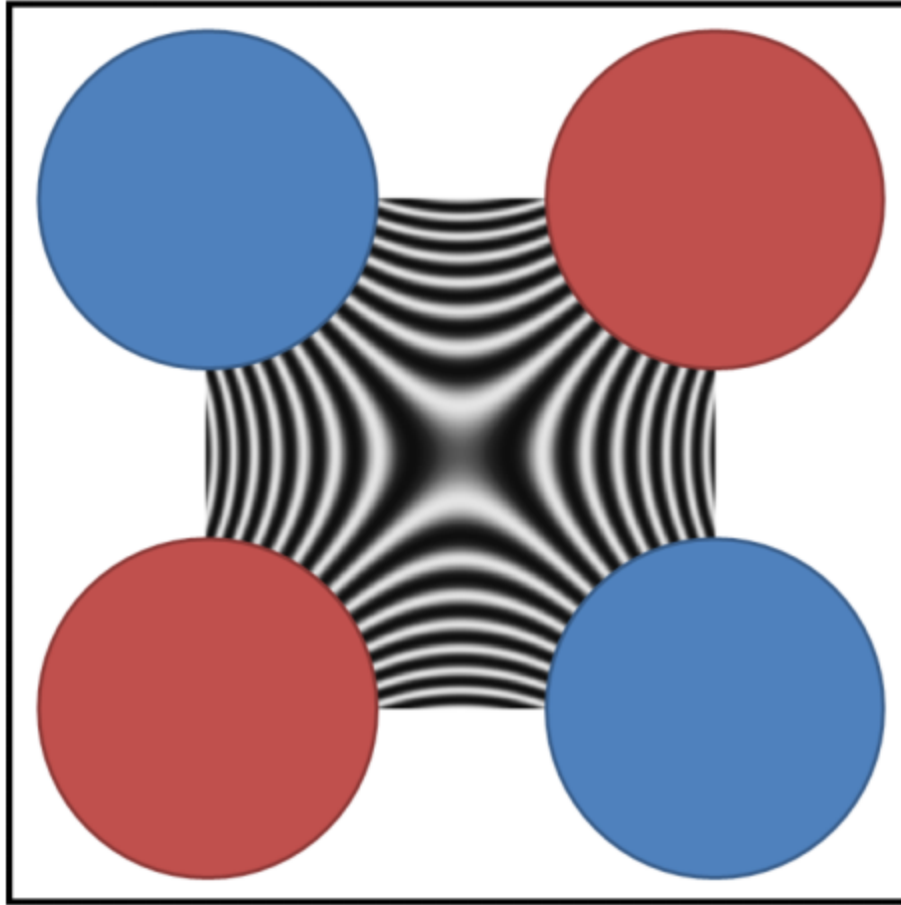


We have a comparison between two scenarios represented in a Figure 9. The first scenario involves the formation of straight isogyres that intersect at the center of the pattern, which occurs when using a sextupolar magnetic field with magnets symmetrically positioned in a circle around the center. The second scenario shows a pattern with curved isogyres, and this occurs when the magnets are symmetrically positioned along an ellipse. Essentially, we have the different light intensities observed under two distinct magnetic field configurations, showing the light intensity zero for the case of isogyres for each region of the light pattern.

These findings indicate that the Mueller matrix used to represent the magnetic field effectively captures the primary features of polarized light intensity in our experiment under both conditions, along with the algebraic properties of the magnetic field.

Although the observed variations in the polar graphs of light intensity could be mitigated by introducing a more intricate angular representation of the magnetic field, for the scope of this study, we successfully illustrated that light intensity at angles associated with isogyre locations is minimized, resulting in darker regions in stark contrast to the brighter areas.

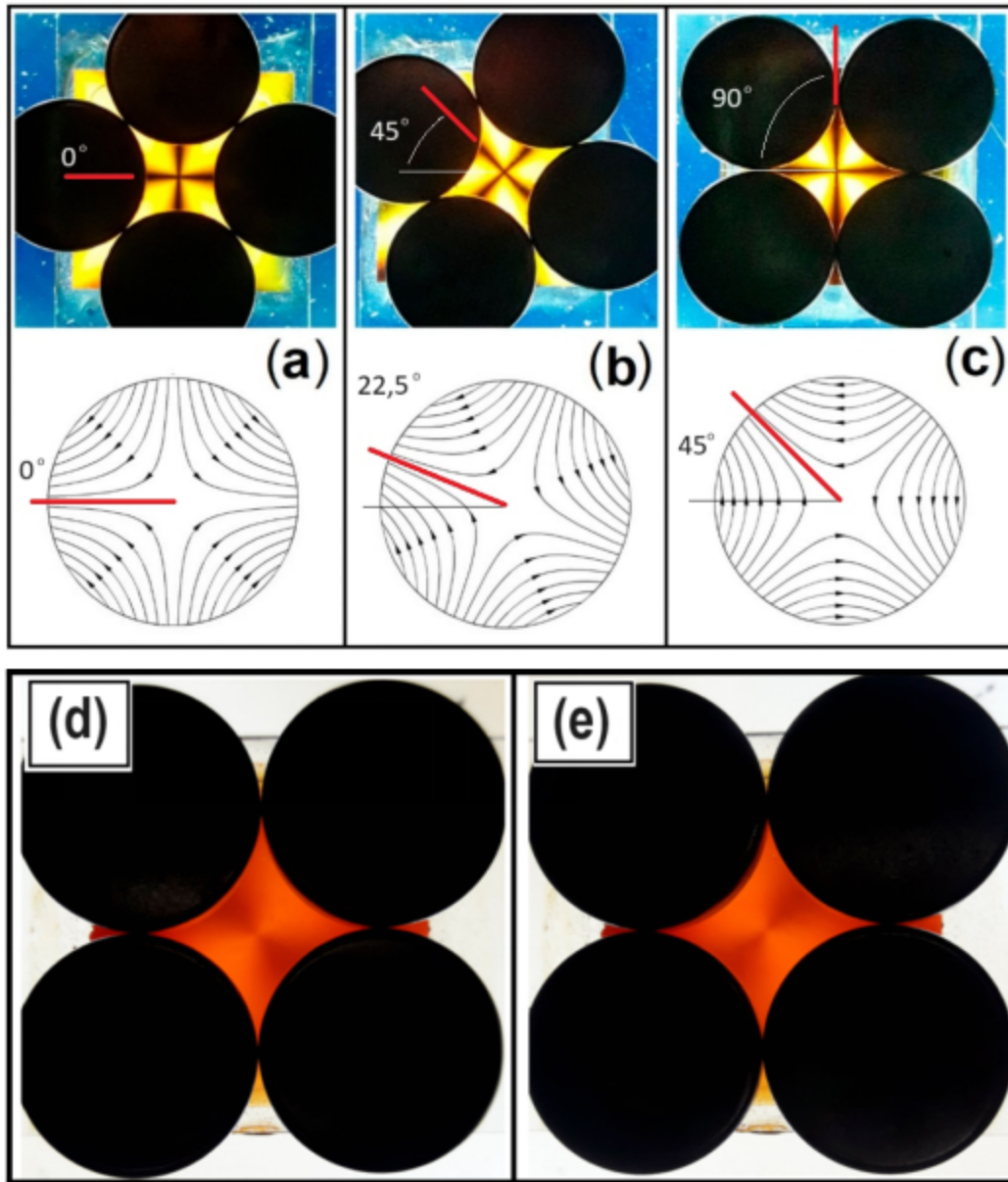
Figure 10
A schematic illustrating the diffraction grating within the quadrupolar field, which will be employed to observe polarization patterns.



A curious case for the rotation of isogyres occur for the case of magnetic quadrupoles. In the presence of a quadrupolar field of Figure 10, the isogyres rotate at twice the angle of the magnetic field, as it is show in Figure 11. The quadrupolar magnetic field in Figure 10 is characterized by parabolic curves around a center in a square arrangement, creating the same effect on the magnetic particles inside the Ferroc cell, and the resulting isogyres are two intersecting lines, forming a cross. The rotation of isogyres in such a field is different from those in other magnetic field configurations.

Figure 11
Creating linearly polarized light within the Ferroc cell under a quadrupole field, we can track the rotation of isogyres as the magnetic field is rotated, as depicted in (a), (b), and (c). Additionally, we observed patterns of light that are circularly polarized to the right in (d) and to the left in (e). The colors displayed indicate varying

intensities, with the highest intensity represented by polarized light in yellow, while circularly polarized light, in red, exhibits lower intensity.



In a quadrupolar field, the arrangement of the diffraction grating is related to a parabolic shape, forming parabolic lines. The polarization of light aligns with these field lines. For a parabola with a mathematical expression like $y(x) = x^2$, the slope of the tangent lines (dy/dx) is given by $2x$. In the context of the quadrupole, this implies that the rotation of the isogyre is directly linked to the rotation of the magnetic field and occurs at twice the rate. This relationship is a consequence of the specific geometric characteristics of the quadrupolar field lines, influencing the behavior of polarized light in the Ferrocell system.

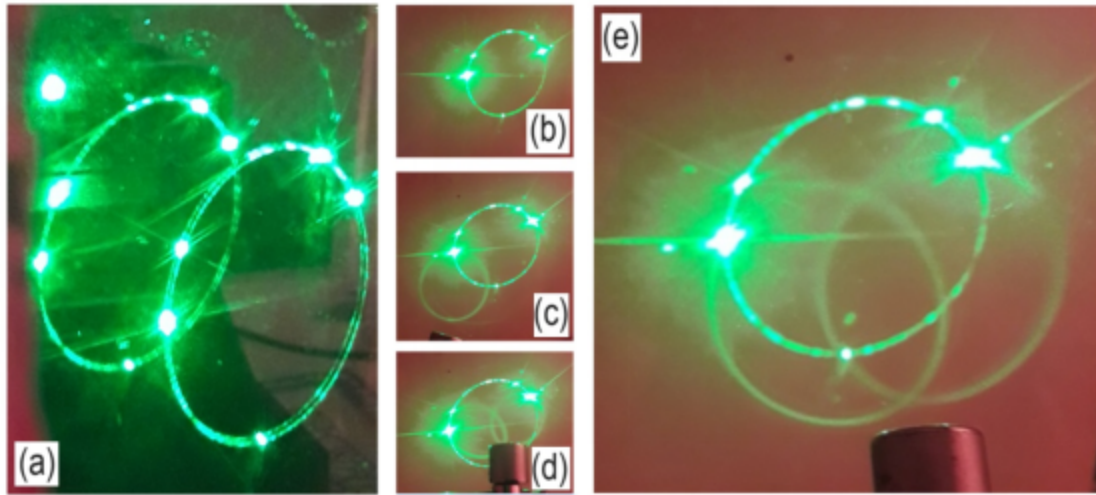
Furthermore, by injecting linearly polarized light into the sample, circularly polarized light patterns were observed, rotating to the right in (d) and to the left in (e). The displayed colors signify different intensities, with yellow indicating the highest intensity for polarized light, while red represents lower intensity for circularly polarized light. This shows that different types of light polarization orientations in ferrofluid thin films can emerge.

4. Parlaseric Circle and Horocycles of Light

While this section does not delve directly into the polarization of light, it highlights intriguing demonstrations of Ferrocell as a magnetic lens and its interactions with sunlight and other light sources, which could lead to future applications in solar panels. We showcase the visualization of a parlaseric circle using the Ferrocell, accompanied by the emergence of luminous horocycles upon the application of a magnetic field. A parlaseric circle (Conover, 2015; Fitzgerald, 2019; Tufaile & Tufaile, 2015) [30-32] is a radiant ring produced by the scattering of light in foams or soap bubbles. This phenomenon is elucidated by the Geometrical Theory of Diffraction (Keller, 1962) [29], shows the phenomenon of reflection and refraction occurring simultaneously, superimposed in a diffraction cone. A parhelic circle shares similarities with the parlaseric circle (Conover, 2015; Fitzgerald, 2019) [30, 31], but manifests in the sky due to light either reflecting or refracting through ice crystals.

Figure 12

Parlaseric circle and the generation of horocycles using Ferrocell. Depictions of the parlaseric circle with a laser beam point and four reflections known as laser dogs are shown in (a). Projection of the parlaseric circle onto a screen is illustrated in (b). The observation of the laser circle through the Ferrocell is demonstrated in (c), and by applying a magnetic field from a magnetic cylinder on the right, the formation of a luminous horocycle at the point corresponding to the laser beam is evident. In (d), with the magnetic cylinder placed more centrally, two small luminous horocycles are observed. When the magnet is positioned lower, two larger luminous horocycles become visible. These images emphasize the interaction between light, magnetic fields, and the unique patterns observed in the context of the Ferrocell experiment.



In the realm of a Ferrocell, a luminous ring known as a horocycle of light can be observed under specific configurations (Tufaile et al., 2021; Bonola, 1955) [34, 35]. In this scenario, the point-shaped source of light partially transforms into a ring perpendicular to the magnetic field. Termed a horocycle of light, this ring bears resemblance to a curve in hyperbolic geometry, where its normal lines asymptotically converge in the same direction. Horocycles are a distinctive feature of hyperbolic geometry, which is a non-Euclidean geometry where the parallel postulate is modified. In hyperbolic geometry, there are no parallel lines, but there are curves like horocycles that exhibit similar geometric properties.

In the context of hyperbolic geometry, a horocycle is a curve with constant curvature, gradually approaching in both directions to a single ideal point. Lobachevsky introduced the terms "horosphere" and "horocycle," revealing their equivalence in geometry to lines and the plane in Euclidean space within hyperbolic settings (Bonola, 1955) [35]. These terms play a crucial role in describing unique structures and patterns in hyperbolic geometry. The notion of a horocycle or horosphere is extensively explored in the field of mathematics (Dani, 1978; Sarnak & Ubis, 2015; Aquino & de Lima, 2014; Colares et al., 2022) [36-39]. Although the concept of a horocycle is not widely explored in physics, it allows us to interpret nonlinear transformations that the magnetic field of a dipole can create in the propagation of light in the Ferrocell. For example, in the realm of general relativity, the connection between relativity and hyperbolic geometry lies in the geometric representation of space-time within the scope of Einstein's theory of General Relativity (Asselmeyer-Maluga & Mader, 2012) [40]. In General Relativity, gravity is described as the curvature of space-time caused by the presence of mass and energy. The mathematics used to describe this curvature is based on the principles of differential geometry, where hyperbolic geometry plays a role. The curvature of space-time affects the

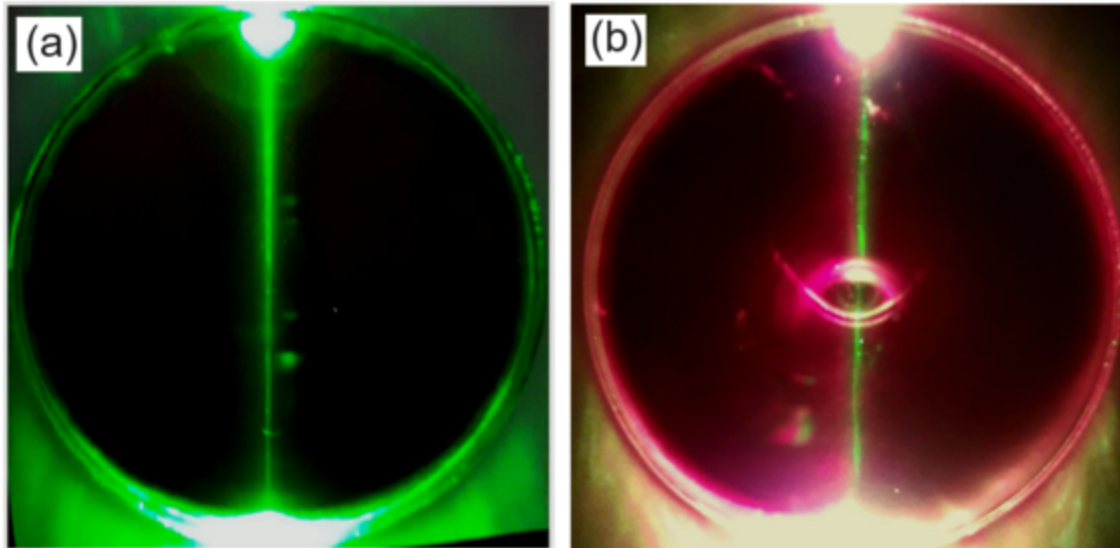
propagation of light. Thinking about a gravitational lens, we can make an analogy here, where the magnetic field in the ferrofluid assumes the same role of the gravitational field in space-time, influencing the propagation of light through the Ferrocell. If we consider that a lens is a transmissive optical device that focuses or disperses a beam of light through refraction, the Ferrocell behaves as if it were partially a magnetic “lens”, as part of the light that passes through it undergoes deviations, such as in the case of refraction, by the nanoparticle structures that align with the magnetic field.

In Figure 12 we show Ferrocell behaving like as a magnetic lens. Figure 12(a) depicts two parlaseric circles projected in a transparent glass. Figure 12 (b) illustrates the observation of the parlaseric circle in the absence of a magnetic field through the magnetic lens. In Figure 12(c) we see the parlaseric circle seen through the magnetic lens with a dipolar magnetic field close to the left side of the parlaseric circle, resulting in the formation of a luminous horocycle, whose origin is related to the most intense luminous point of the parlaseric circle, which corresponds to the laser beam. In Figure 12(d), the dipole field is shifted and is applied to the lower central part of the parlaseric circle, leading to the observation of two luminous horocycles, one due to the laser beam and the other due to a laser dog. Two large horocycles are shown in Figure 12(e).

In the observed projections of the diffraction circle which forms the parlaseric circle, five luminous points are identified. The leftmost point represents the laser beam interacting with the Plateau border, while the other points on the circle represent the laser dogs (Conover, 2015) [30], which are reflections of the laser beam. Luminous horocycles primarily emerge in regions with intense light signals, particularly at points characterized by a robust laser reflection from the Plateau border and the position corresponding to the laser beam.

Figure 13

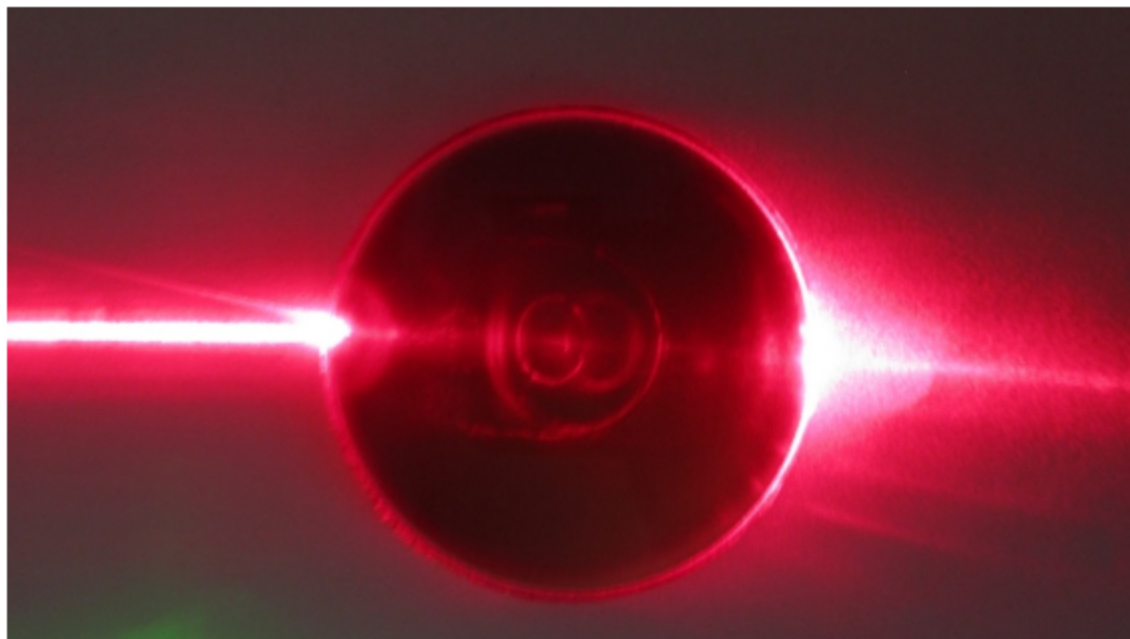
In (a), a green laser beam is directed towards the edge of a circular Ferrocell with no magnetic field. In (b), a red beam and a green beam are directed towards the edge of the Ferrocell in the presence of a monopolar magnetic field, which means that one pole of a cylindrical magnet is in contact with the center of the plate behind it. The magnet remains unseen due to an opaque sheet positioned between it and the Ferrocell. The observed pattern is solely attributed to the magnetic field within the Ferrocell scattering the laser beam.



The creation of luminous horocycles represents a specific instance of image generation within the fluid. This can be verified by introducing a laser beam directly into the Ferrocell and implementing a magnetic field. In Figure 13 and Figure 14, we observe patterns within the Ferrocell. Due to the presence of phenomena associated with the Geometric Theory of Diffraction (GTD) (Keller, 1962) [29] in the Ferrocell, these effects might be mistakenly perceived as a mere reflection. However, the system experiences a multifaceted interplay between light and nanoparticles, resulting in a phenomenon encompassing both reflection/refraction and diffraction simultaneously. The competition between the effects of diffraction and reflection/refraction in the Ferrocell depends on the intensity of the light seen through it and the contrast between other nearby light sources. In this context, we acknowledge that the Ferrocell exhibits optical phenomena situated at the intersection of geometric optics and wave optics. To comprehend the intricate patterns it produces, one must factor in the dual nature of light, behaving simultaneously as both a wave and a ray, a phenomenon known as wave-ray duality in classical physics, analogous the wave-particle duality in quantum mechanics.

Figure 14

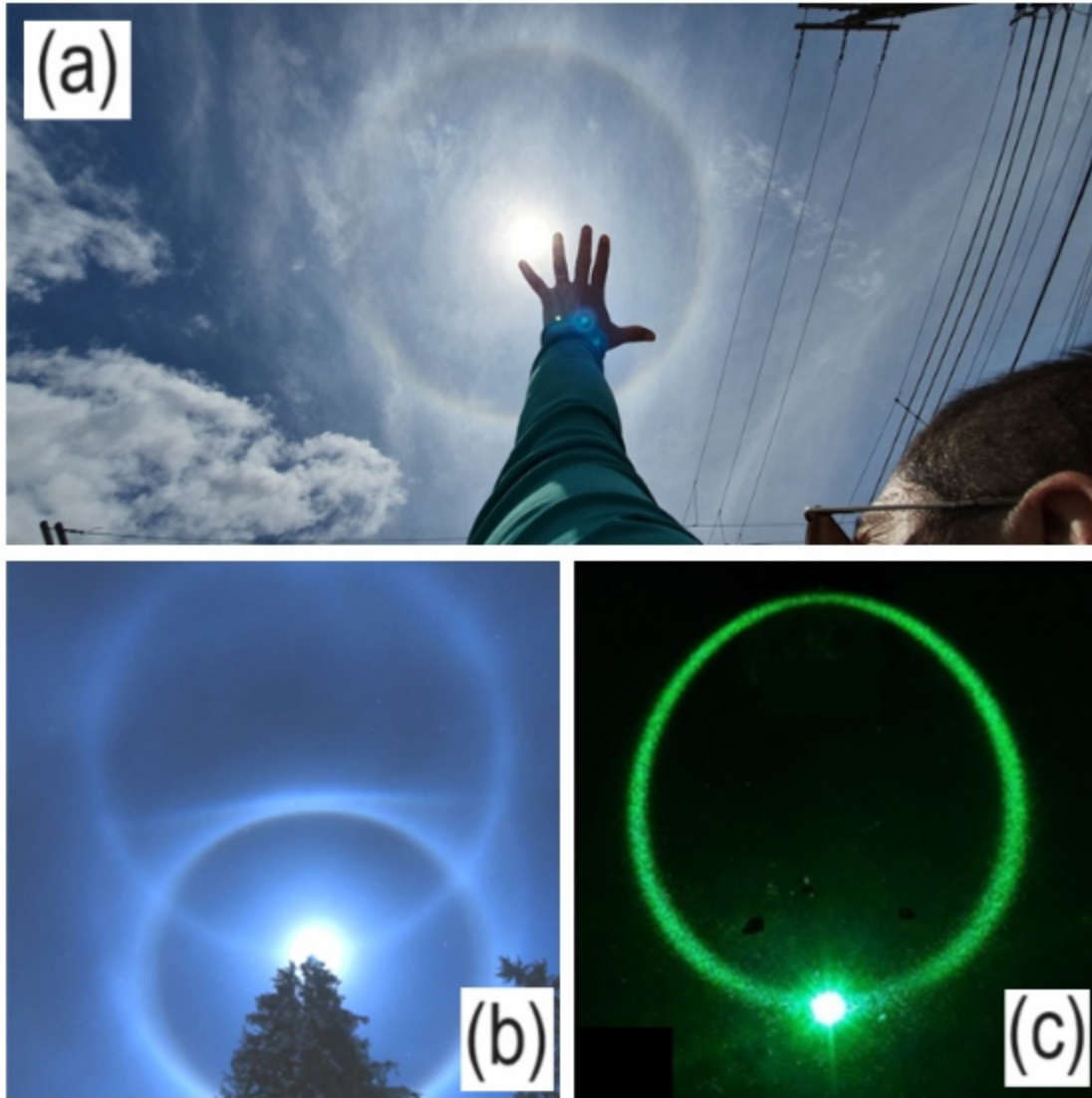
A red laser beam directed into the edge of the Ferrocell under a stronger monopolar magnetic field behind it. The magnet remains unseen due to an opaque sheet positioned between it and the Ferrocell. The observed pattern is solely attributed to the magnetic field within the Ferrocell scattering the laser beam.



This experiment reveals that employing diverse analysis techniques from various areas of physics enables the discovery of connections with abstract mathematical concepts, particularly those related to topology. Additionally, it establishes links with the studies associated with other smart materials, as exemplified in the examination of light propagation within systems involving liquid crystals (Kamien & Machon, 2020; Pollard & Alexander, 2021) [41, 42]. This suggests a potential avenue for utilizing this device in the exploration of applications within display technology. Following this idea of using the concepts learned with Ferrocell in other areas, understanding the phenomena in this section allows us to try to understand other phenomena that can be observed in atmospheric optics.

Figure 15

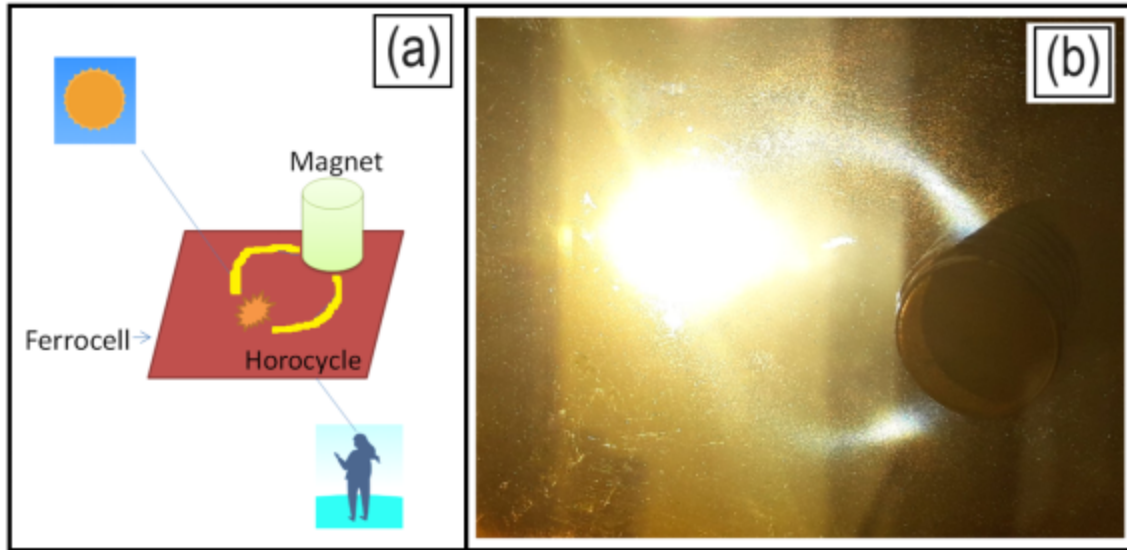
Pattern formation involving different type of ice crystals geometries. In (a), the author extends her arm with an open hand to visually demonstrate the solid angle of the 22-degree solar halo. In (b), alongside the solar halo, the parhelic circle is depicted. In (c), a luminous horocycle, generated using a Ferrocell, is presented.



We have expanded the application of generating diverse magnetic field configurations to elucidate pattern formation in atmospheric optics. This involves drawing an analogy between the size of structures in ferrofluid and ice crystals present in the atmosphere. For instance, in Figure 15(a), we observe geometric optical effects contributing to the formation of the 22° solar halo, centered around the sun. In Figure 15(b), alongside the solar halo, the parhelic circle intersects the sun, similar to the luminous horocycle illustrated in Figure 15(c).

Figure 16

Diagram illustrating the Ferrocell and a magnet demonstration to generate a horocycle, utilizing the sun as the light source in (a). In (b), a photograph capturing this experiment.



In Figure 16, we showcase an experiment demonstrating the creation of a horocycle pattern using the sun as a light source in the presence of a magnetic field. In Figure 16(a), we present the diagram of this demonstration, positioning the Ferrocell between the observer and the sun. Figure 16(b) displays an image captured with this configuration. It is noteworthy that the luminous horocycle intersect at the sun, similar to the parhelic circle.

5. Conclusions

In conclusion, this study provides a comprehensive exploration of the intricate interplay between magnetic fields and light polarization within thin films of ferrofluid. Leveraging the Ferrocell device and employing advanced techniques like polarized light imaging, multipolar expansion, and Mueller matrix formalism, the research investigated the formation of isogyres, which are distinct patterns observed during the passage of polarized light through ferrofluid under diverse magnetic field configurations. The alignment of nanoparticles in response to the magnetic field leads to the creation of a diffraction grating, influencing light polarization. Utilizing Stokes vectors, Mueller matrices, and multipolar expansion, the study sheds light on the complex relationship between magnetic fields and optical properties in ferrofluid thin films.

Our experiment also showcased the evolution of isogyres from straight lines to conic projections, such as parabolas and hyperbolas, under the influence of a monopolar, dipolar, quadrupolar and sextupolar magnetic fields. The Mueller matrix effectively represented the magnetic field's impact on polarized light, revealing dark regions corresponding to isogyres. These findings contribute to a nuanced understanding of how magnetic fields shape light polarization in ferrofluid thin films, holding potential applications in magneto-optical devices, materials science, and biomedical imaging. The use of polarization patterns through their isogyres to represent magnetic fields is an interesting way to have a new perspective on the representation of vector fields.

Additionally, the study presents the visualization of a parhelic circle through the Ferrocell, illustrating the formation of luminous horocycles. Using the Ferrocell, we have observed a luminous horocycle. In this phenomenon, a point light source is transformed into a ring perpendicular to the magnetic field in the plane of the Ferrocell. This work opens avenues for further exploration and application of these phenomena in diverse scientific and technological domains, like the case of the solar panels.

Ethical Statement

This study does not contain any studies with human or animal subjects performed by any of the authors.

Conflicts of Interest

The authors declare that they have no conflicts of interest to this work.

References

1. Tufaile, A., Vanderelli, T. A., Snyder, M., & Tufaile, A. P. B. (2019). Observing dynamical systems using magneto-controlled diffraction. *Condensed Matter*, 4(2), 35. <https://doi.org/10.3390/condmat4020035>
2. Haas, W. E., & Adams, J. E. (1975). Diffraction effects in ferrofluids. *Applied Physics Letters*, 27(10), 571-572. <https://doi.org/10.1063/1.88299>
3. Mendeleev, V. S., & Ivanov, A. O. (2004). Ferrofluid aggregation in chains under the influence of a magnetic field. *Physical Review E*, 70(5), 051502. <https://doi.org/10.1103/PhysRevE.70.051502>
4. Ivanov, A. O., & Zubarev, A. (2020). Chain formation and phase separation in ferrofluids: The influence on viscous properties. *Materials*, 13(18), 3956. <https://doi.org/10.3390/ma13183956>
5. Horng, H. E., Hong, C. Y., Yang, S. Y., & Yang, H. C. (2003). Designing the refractive indices by using magnetic fluids. *Applied Physics Letters*, 82(15), 2434-2436. <https://doi.org/10.1063/1.1568147>
6. Martínez, L., Cecelja, F., & Rakowski, R. (2005). A novel magneto-optic ferrofluid material for sensor applications. *Sensors and Actuators A: Physical*, 123, 438-443.
7. Candiani, A., Margulis, W., Sterner, C., Konstantaki, M., & Pissadakis, S. (2011). Phase-shifted Bragg microstructured optical fiber gratings utilizing infiltrated ferrofluids. *Optics letters*, 36(13), 2548-2550. <https://doi.org/10.1364/OL.36.002548>
8. Thakur, H. V., Nalawade, S. M., Gupta, S., Kitture, R., & Kale, S. N. (2011). Photonic crystal fiber injected with Fe₃O₄ nanofluid for magnetic field detection. *Applied Physics Letters*, 99(16), 161101. <https://doi.org/10.1063/1.3651490>
9. Zu, P., Chan, C. C., Lew, W. S., Hu, L., Jin, Y., Liew, H. F., ... & Dong, X. (2012a). Temperature-insensitive magnetic field sensor based on nanoparticle magnetic fluid and photonic crystal fiber. *IEEE photonics journal*, 4(2), 491-498.
10. Zu, P., Chan, C. C., Lew, W. S., Jin, Y., Liew, H. F., Chen, L. H., ... & Dong, X. (2012b). High extinction ratio magneto-optical fiber modulator based on nanoparticle magnetic fluids. *IEEE Photonics Journal*, 4(4), 1140-1146.
11. Li, J., Wang, R., Wang, J., Zhang, B., Xu, Z., & Wang, H. (2014). Novel magnetic field sensor based on magnetic fluids infiltrated dual-core photonic crystal fibers. *Optical Fiber Technology*, 20(2), 100-105.
12. Li, Y., Pu, S., Hao, Z., Yan, S., Zhang, Y., & Lahoubi, M. (2021). Vector magnetic field sensor based on U-bent single-mode fiber and magnetic fluid. *Optics Express*, 29(4), 5236-5246.
13. Cennamo, N., Arcadio, F., Marletta, V., Baglio, S., Zeni, L., & Andò, B. (2020). A magnetic field sensor based on SPR-POF platforms and ferrofluids. *IEEE Transactions on Instrumentation and Measurement*, 70, 1-10. <https://doi.org/10.1109/TIM.2020.3035114>
14. Gao, T. Y., Ma, G. M., Wang, Y. K., Gao, D., Qin, W. Q., Wang, Y., & Yan, C. (2022). Effect of Structure on Sensitivity of Magnetic Field Sensor Based on Non-Adiabatic Tapered Optical Fiber With Magnetic Fluid. *IEEE Sensors Journal*, 22(5), 4022-4027. doi: 10.1109/JSEN.2022.3142313.
15. Chen, Y., Zhang, X., Zhang, Q., Wang, Z., Fei, J., Yang, Y., ... & Wang, T. (2023). All-optical tuning of microbottle resonator assisted by a movable probe with magnetic nanoparticles. *IEEE Sensors Journal*, 23(22), 27416-27422. doi: 10.1109/JSEN.2023.3323009
16. Dave, V., Mehta, R. V., & Bhatnagar, S. P. (2020). Extinction of light by a Ferrocene and ferrofluid layers: A comparison. *Optik*, 217, 164861. doi: 10.1016/j.ijleo.2020.164861.
17. Chen, Q., Wang, H., Wang, Q., & Pan, Y. (2018). Plasmon Enhanced Faraday Rotation in Fe₃O₄/Ag Ferrofluids for Magneto Optical Sensing Applications. *Plasmonics*, 13, 353-363. <https://doi.org/10.1007/s11468-017-0606-1>.
18. Fan, F., Zhong, C., Zhang, Z., Li, S., & Chang, S. (2021). Terahertz chiral sensing and magneto-optical enhancement for ferromagnetic nanofluids in the chiral metasurface. *Nanoscale Advances*, 3(16), 4790-4798.
19. Minuti, A. E., Stoian, G., Herea, D. D., Radu, E., Lupu, N., & Chiriac, H. (2022). Fe-Cr-Nb-B ferrofluid for biomedical applications. *Nanomaterials*, 12(9), 1488. doi: 10.3390/nano12091488.
20. Shokrollahi, H. (2013). Structure, synthetic methods, magnetic properties and biomedical applications of ferrofluids. *Materials Science and Engineering: C*, 33(5), 2476-2487. doi: 10.1016/j.msec.2013.03.028.
21. Gu, Y., Valentino, G., & Mongeau, E. (2014). Ferrofluid-based reconfigurable optofluidic switches for integrated sensing and digital data storage. *Applied Optics*, 53(4), 537-543.
22. Mansuori, M., Zareei, G. H., & Hashemi, H. (2015). Reconfigurable optofluidic switch for generation of optical pulse width modulation based on tunable reflective interface. *Applied optics*, 54(28), E63-E68.
23. Samlan, C. T., Naik, D. N., & Viswanathan, N. K. (2016). Isogyres – Manifestation of Spin-orbit interaction in uniaxial crystal: A closed-fringe Fourier analysis of conoscopic interference. *Scientific Reports*, 6(1), 33141. doi: 10.1038/srep33141.
24. Kamb, W. B. (1958). Isogyres in interference figures. *American Mineralogist: Journal of Earth and Planetary Materials*, 43(11-12), 1029-1067.

25. Victor, A. E., & Beyer, R. T. (1973). Ultrasonic absorption measurements in oriented benzene crystals. *The Journal of the Acoustical Society of America*, 54(6), 1639-1650. doi: 10.1121/1.1914462.
26. Berry, M., Bhandari, R., & Klein, S. (1999). Black plastic sandwiches demonstrating biaxial optical anisotropy. *European Journal of Physics*, 20(1), 1-14. <https://michaelberryphysics.files.wordpress.com/2013/07/berry303.pdf>
27. Kompaneitsev, V. P. (2006). Isogyre equation for uniaxial and biaxial crystals. *Crystallography Reports*, 51, 640-645. <https://doi.org/10.1134/S1063774506040171>
28. Samlan, C. T., Naik, D. N., & Vishwanathan, N. K. (2016, December). Separating isogyres and isochromates of a uniaxial crystal using Fourier fringe analysis. In *International Conference on Fibre Optics and Photonics* (pp. Th3A-4). Optica Publishing Group. <https://doi.org/10.1364/PHOTONICS.2016.Th3A.4>
29. Keller, J. B. (1962). Geometrical theory of diffraction. *JOSA*, 52(2), 116-130. doi: 10.1364/josa.52.000116. PMID: 14454948.
30. Conover, E. (2015). Researchers create 'laser dogs' with soap bubbles. *Science Magazine*. <http://dx.doi.org/10.1126/science.aaa7816>
31. Fitzgerald, R. J. (2019). Soap halos. *Physics Today*, 72(7), 68. <https://doi.org/10.1063/PT.3.4257>
32. Tufaile, A., & Tufaile, A. P. B. (2015). The dynamics of diffracted rays in foams. *Physics Letters A*, 379(47-48), 3059-3068. doi: 10.1016/j.physleta.2015.10.011.
33. Tufaile, A., & Tufaile, A. P. B. (2022). Exploring the Polarization of Light in Ferrofluids with Mueller Matrices. *Magnetochemistry*, 8(10), 121. doi: 10.3390/magnetochemistry8100121.
34. Tufaile, A., Snyder, M., & Tufaile, A. P. B. (2021). Horocycles of Light in a Ferrocylinder. *Condensed Matter*, 6(3), 30. <https://doi.org/10.3390/condmat6030030>
35. Bonola, R. (1955). *Non-Euclidean geometry: A critical and historical study of its development*. Courier Corporation.
36. Dani, S. G. (1978). Invariant measures of horospherical flows on noncompact homogeneous spaces. *Inventiones mathematicae*, 47(2), 101-138. <https://doi.org/10.1007/BF01578067>
37. Sarnak, P., & Ubis, A. (2015). The horocycle flow at prime times. *Journal de mathématiques pures et appliquées*, 103(2), 575-618.
38. Aquino, C. P., & de Lima, H. F. (2014). On the geometry of horospheres. *Commentarii Mathematici Helvetici*, 89(3), 617-629. doi: 10.4171/CMH/329
39. Colares, A. G., de Lima, H. F., & Velásquez, M. A. L. (2022). Revisiting the geometry of horospheres of the hyperbolic space. *Monatshefte für Mathematik*, 199(4), 771-784. <https://doi.org/10.1007/s00605-022-01758-2>
40. Asselmeyer-Maluga, T., & Mader, R. (2012, February). Exotic R4 and quantum field theory. In *Journal of Physics: Conference Series*, 343(1), 012011. DOI 10.1088/1742-6596/343/1/012011
41. Kamien, R. D., & Machon, T. (2020). Geodesic fibrations for packing diabolic domains. *Proceedings of the National Academy of Sciences*, 117(39), 24102-24109. <https://doi.org/10.1073/pnas.2014402117>
42. Pollard, J., & Alexander, G. P. (2021). Intrinsic geometry and director reconstruction for three-dimensional liquid crystals. *New Journal of Physics*, 23(6), 063006. <https://doi.org/10.1088/1367-2630/abfd4>

How to Cite:

Tufaile, A. & Tufaile, A. P. B. (2024) Investigating Isogyres in Ferrofluids and Horocycles from Parabolic Circle in a Ferrocylinder. *Journal of Optics and Photonics Research*. <https://doi.org/10.47852/bonviewJOPR42022329>